13 (2023) 100308

Contents lists available at ScienceDirect

Biosensors and Bioelectronics: X

journal homepage: www.journals.elsevier.com/biosensors-and-bioelectronics-x

Rapid assessment of antibiotic susceptibility using a fully 3D-printed impedance-based biosensor

R. Domingo-Roca [a,*], P. Lasserre [a], L. Riordan [b], A.R. Macdonald [a], A. Dobrea [a], K.R. Duncan [b], S. Hannah [a], M. Murphy [c], P.A. Hoskisson [b], D.K. Corrigan [d]

[a] Department of Biomedical Engineering, University of Strathclyde, 106 Rottenrow East, Glasgow, G4 0NW, United Kingdom
[b] Strathclyde Institute of Pharmacy & Biomedical Sciences, University of Strathclyde, 161 Cathedral Street, Glasgow, G4 0RE, United Kingdom
[c] Department of Medical Microbiology, New Lister Building, Glasgow Royal Infirmary, 84 Castle Street, Glasgow, G4 0SF, UK
[d] Department of Pure and Applied Chemistry, Thomas Graham Building, 295 Cathedral Street, Glasgow, G1 1XL, UK

ARTICLE INFO

Keywords:
3D-printing
Electrochemical biosensor
Escherichia coli
Pseudomonas aeruginosa
Antimicrobial resistance
Growth profiles

ABSTRACT

The sustained misuse and overuse of antibacterial agents is accelerating the emergence of antimicrobial resistance (AMR), which is becoming one of the major threats to public health. Abuse of antibiotics drives spontaneous evolution, bacterial mutation, and exchange of resistant genes through lateral gene transfer. Mitigating the worldwide impact of AMR requires enhanced antibiotic stewardship through faster diagnostic testing. In this work, we aim to tackle this issue via development of a fully 3D-printed electrochemical, gel-modified biosensor for rapid bacterial growth monitoring. By using electrochemical impedance spectroscopy, we have successfully identified growth profiles and confirmed antibiotic susceptibility of two ESKAPE pathogens, *Escherichia coli* and *Pseudomonas aeruginosa*, following overnight culture it was possible to determine antibiotic sensitivity in 90 min, altogether faster than the 24–48 h current gold standard of culture-based antimicrobial susceptibility testing with significant scope for optimisation. Results show a clear distinction between growth profiles in the presence and absence of amoxicillin, gentamicin, and fosfomycin, therefore demonstrating a rapid, cost-efficient platform for phenotypic antibiotic susceptibility testing within clinically relevant concentration ranges for conditions such as urinary tract infections and pneumonia.

1. Introduction

Antimicrobial resistance (AMR) occurs when microorganisms adapt and grow in the presence of agents that had once inhibited their growth. Bacteria, fungi, parasites, and viruses can all develop AMR, and the fact that the infectious diseases they cause can no longer be treated with antimicrobials, is one of the biggest threats to public health. AMR currently accounts for 1.27 million deaths per year worldwide (Murray et al., 2022) and it is expected to reach 10 million annual cases by 2050 if measures are not put in place (O'Neill, 2014). Current routine practices take, at least, 48 h to assess the optimum antibiotic to treat a specific infection, therefore increasing the chances of the patient developing further complications. For instance, bacterial infections are the most common cause of sepsis, which is one of the leading sources of morbidity and mortality in low- and middle-income countries (LMIC (Kodan et al., 2018),), and with each hour treatment is delayed, sepsis survival reduces by 7.6% (Kumar et al., 2006). It is crucial to develop technologies to help rapid and reliable assessment of AMR, such that identification of both the type of infection (bacterial or nonbacterial) and the most adequate treatment can be provided to the patient.

In order to address such a broad issue, the World Health Organization (WHO) adopted a global action plan in 2015 on antimicrobial resistance, launching a call for the so-called One Health approach (World Health Organization, 2015). One of the objectives of this call is to increase investment in diagnostic tools such that AMR can be detected and treated as fast as possible. Nevertheless, the current gold standard for antibiotic susceptibility testing still relies on traditional microbiology approaches, where a sample is cultured and examined through staining and optical techniques. This process takes, at least, 2 days to provide information about the infection, which can easily take longer in slower-growing organisms such as *Mycobacterium tuberculosis* (Gumbo et al., 2009; Musuka et al., 2013). These prolonged diagnostic times lead to delayed treatments, which can increase bacterial resistance or even become fatal in time-limited scenarios. To accelerate this process, there

* Corresponding author.106 Rottenrow East, Glasgow, G4 0NW, United Kingdom.
E-mail address: roger.domingo-roca@strath.ac.uk (R. Domingo-Roca).

https://doi.org/10.1016/j.biosx.2023.100308
Received 11 November 2022; Received in revised form 12 January 2023; Accepted 23 January 2023
Available online 1 February 2023

have been a set of automated approaches put in place to assess AMR, and 4 of them have been cleared by the U.S. Food and Drug Administration. While promising, these methods still require standardised microbial inoculum (post 24–48 h culture, if not longer) and dense bacterial suspensions (van Belkum et al., 2020). New technologies have been developed and investigated to reduce these long diagnostic times, including machine learning and artificial intelligence-based methods (Anahtar et al., 2021; Baltekin et al., 2017; Elyan et al., 2022; Khaledi et al., 2020), microfluidic-optical coupled systems (Qiu and Nagl, 2021; Son and Stocker, 2019; Vasala et al., 2020), mechanical approaches (Etayash et al., 2016; Johnson et al., 2017), and chemical methods (Derzsi et al., 2016; Tang et al., 2013). While some of these approaches are highly sensitive, they are limited by their complexity and cost (Behera et al., 2019), therefore becoming unavailable worldwide or requiring specialised equipment and training.

Electrochemical approaches have arisen as one of the most promising techniques for rapid, cost-efficient evaluation of cellular growth in bacteriological samples (Brosel-Oliu et al., 2019a; Gnaim et al., 2020; Hannah et al., 2020a, 2022; Wang et al., 2021). Electrochemical impedance spectroscopy (EIS) is a very powerful tool since it evaluates the impedance of a sample across a range of frequencies. These impedimetric measurements contain information about the resistive and reactive components of the sample, which can be monitored over time through sequential measurement and be used to induce bacterial growth and growth inhibition (Brosel-Oliu et al., 2019a; Hannah et al., 2020a; Ward et al., 2018). By controlling impedance evolution over time, EIS has already demonstrated successful detection of *Staphylococcus aureus*, *Escherichia coli*, and *Pseudomonas aeruginosa*, as well as it has allowed to discern between oxacillin-susceptible and resistant strains of *S. aureus* (Hannah et al., 2019) (further examples including time-to-result are shown in Table 1). One of the few limitations of using this approach is that EIS studies are traditionally performed using commercially-available screen-printed electrodes (SPEs), which offer a number of advantages over conventional diagnostics tools, but also have a set of disadvantages such as a non-customisable design, cost-inefficient large production, and their long-term use may be sparse especially in resource-limited settings. Several groups have addressed this issue by 3D-printing their own diagnosis and analysis systems, but most of them still rely on commercially-available SPEs, overnight cultured samples, and/or use traditional analytical tools (Brosel-Oliu et al., 2019a; Ramiah Rajasekaran et al., 2020; Rengaraj et al., 2018; Sebechlebská et al., 2022; Siller et al., 2020). Further exploitation of 3D-printing and production of personalised electrodes using conductive materials has already proved to be highly useful to develop various electrochemical devices. Some of them are able to measure several substances such as pyoverdine, glucose, dopamine, ascorbic acid, and a long list of other life-relevant molecules (Cardoso et al., 2020; Hatada et al., 2018; Manzanares Palenzuela et al., 2018; McLean et al., 2022; Richter et al., 2019). The ability to 3D-print fully personalised electrochemical sensors allows for full control over their design, therefore improving their sensitivity to a specific analyte of interest. Nevertheless, to the best of our knowledge, functional multi-material 3D-printing has not yet been exploited for production of gel-modified impedimetric biosensors per se, including both testing platform and electrode.

Table 1
Bacterial strains and time-to-result in impedimetric biosensors from the literature.

Strain	Time to result	Overnight culture/other +24 pre-test conditions?	Reference
E. coli *P. aeruginosa* *S. aureus* *C. albicans*	24 h	Not stated	Martins and Selby (1980)
P. putida	24 h	YES	Miller et al. (2019)
B. lactis	8–9 h	YES	Walker et al. (2005)
L. innocua	7–9 h	YES	Felice et al. (1999)
L. innocua *E. coli* *L. monocytogenes*	2–4 h	YES	Gómez (2002)
E. coli	60 min	YES	Butler et al. (2019)
E. coli	~60 min	YES	Brosel-Oliu et al. (2019b)
S. typhis *S. aureus*	30–60 min	NO (12 h–15 h)	Swami et al. (2021)
S. typhimurium *E. coli* *L. pneumonophila*	30–40 min	YES	Muhsin et al. (2022)
E. coli *S. aureus* *K. pneumoniae*	30 min	NO (12 h–15 h)	Swami et al. (2022)

Our previous work demonstrated that (i) functionalisation of SPEs through gel modification improves the measurement duration and can detect a range of microorganisms (Hannah et al., 2019, 2020b), and (ii) it is possible to exploit multi-material 3D-printing to produce one-step, portable electrochemical devices to reliably detect a series of redox analytes and life-relevant molecules such as dopamine and glucose (Domingo-Roca et al., 2022). In this work, we combine these two concepts into a novel and rapid approach to antimicrobial susceptibility testing (AST) determination via an impedimetric biosensor. We additionally introduce a new protocol to analyse the obtained data and induce relative bacterial growth and growth inhibition through investigation of doubling times over a range of frequencies. This approach allows for correlation of a set of variables (impedance, resistance, reactance, and negative phase) on bacterial growth and inhibition in under 90 min. We demonstrate the validity of this method by analysing how trimethoprim-susceptible and resistant strains of *E. coli* (UPEC-29 and UPEC-3, respectively) and of gentamicin-susceptible and resistant *P. aeruginosa* (PA14, and LESB58, respectively) respond to a set of different antibiotics (trimethoprim, amoxicillin, gentamicin, and fosfomycin) with sampling size (N) of 3 (unless otherwise stated) to ensure data reliability. Our customised 3D-printed electrochemical platform allows for the deposition of enough gel (70 μL) and sample volume (100 μL) to avoid gel and sample evaporation and obtain reliable growth and inhibition profiles (Fig. 1). We decided to use these quantities to ease use of the platform in non-specialised settings, since these amounts are convenient for standard lab-based pipette tip sizes. The ability to 3D-print fully personalised biosensors is demonstrated to be an extremely powerful tool in research settings since it allows researchers to try out different designs in a time- and cost-effective manner to speed up the time for new designs to be tested.

2. Materials and methods

2.1. 3D-Printing

Multi-material 3D-printed sensors were produced as previously described (Domingo-Roca et al., 2022). Briefly, a portable electrochemical biosensor including reference, counter, and working electrodes was 3D-printed in a RAISE3D-E2 IDEX Dual 3D printer (nozzle diameter 0.4 mm) using polylactic acid (PLA, RAISE) as main housing, and carbon black PLA (CB-PLA, ProtoPasta) for the electrodes. The electrochemical sensor features a well on top of the electrodes where the gel is deposited and, after gelation, the sample is placed on top. Dynamic bacterial metabolic processes induce a set of electron exchange processes that are monitored by the sensor using impedance measurements (schematic in Fig. 1).

2.2. Electrode surface cleaning

All 3D-printed electrodes were treated with an oxygen plasma

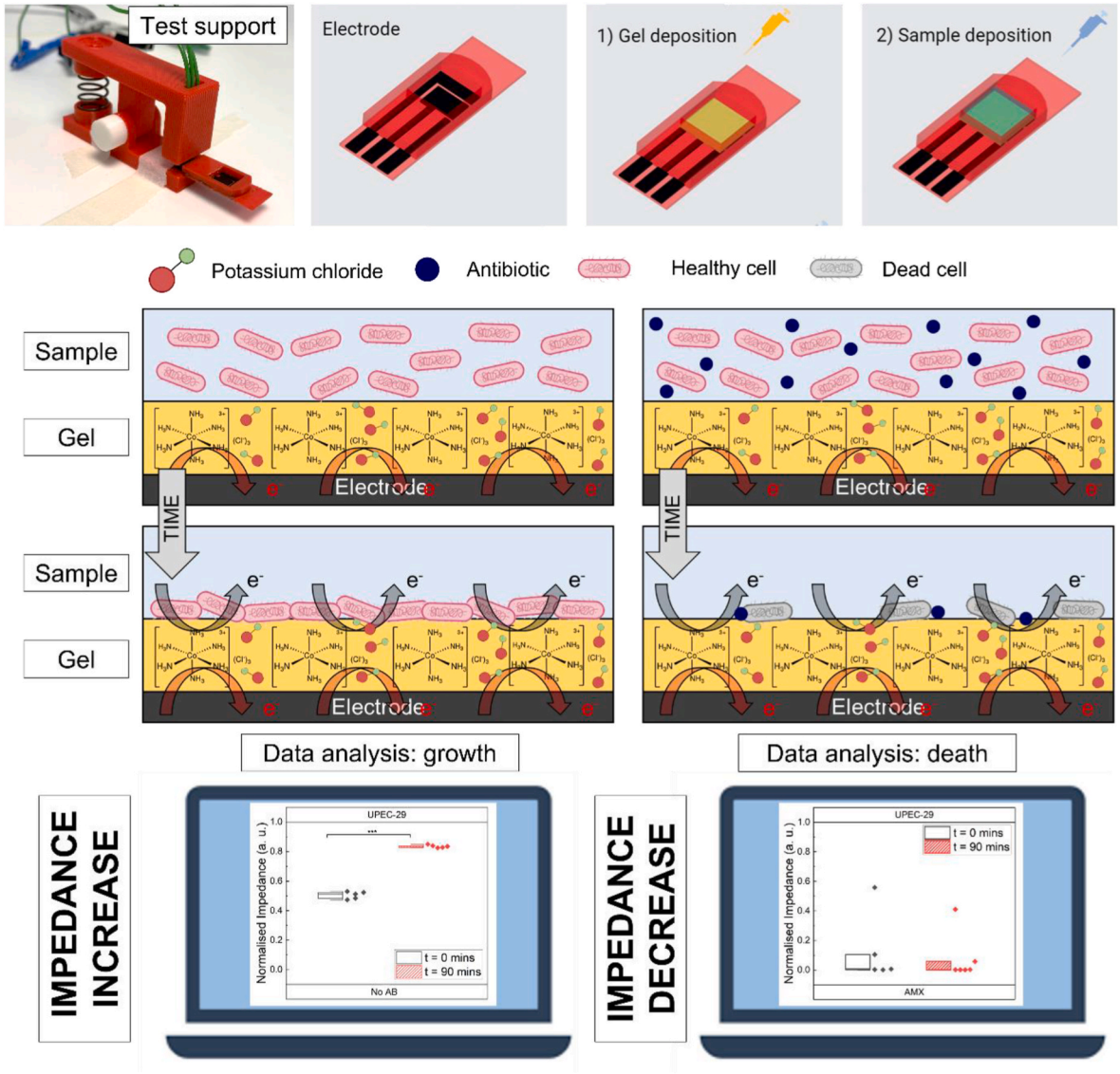

Fig. 1. The top left-hand side panel shows a picture of the experimental set up used in this work prior to gel and sample deposition. The other three images on the top row show a schematic of the preparation of the gel-modified 3D-printed electrode, where the hexaammineruthenium (IIII) chloride gel (2 mM) is deposited. After gelation, the sample containing the bacteria is deposited on top. The panels below show a schematic of the gel formulation and how the metabolic bacterial processes generate an electron exchange that is measured in impedance format using the electrode both in the presence and absence of antibiotic.

cleaning and surface activation protocol. Plasma cleaning was conducted in a Zepto Diener chamber (Diener Electronic, GmbH, Ebhausen, Germany) and running a standard cleaning protocol with chamber pressure 0.3 mbar, O_2 flow rate of 0.25 Nl/h, a power setting of 65% (130 W), and a process time of 1 min. Following this, an additional electrochemical cleaning process was performed by cycling 10 times in 1 M sulfuric acid (H_2SO_4) between −1.5 V and 1 V at 300 mV/s. After H_2SO_4 cleaning, the electrodes were gently rinsed with de-ionised water and dried in Ar.

2.3. Gel preparation and deposition on 3D-printed electrode

2 mM hexaammineruthenium (III) chloride (HexRu, Merck, UK) gels were prepared in a two-step process. Firstly, a 1% w/v agarose (Fisher Bioreagents, UK), 2.5% w/v Miller Lysogeny (LB) Broth (Fisher Bioreagents, UK), and 97 mM potassium chloride (KCl, Merck, UK) solution was prepared in 100 mL of 18.2 MΩ de-ionised water (ELGA LabWater PURELAB Chorus), autoclaved at 121 °C for 20 min, and stored at 4 °C until use. HexRu-loaded gels were prepared in small batches in a sterile environment by adding 3.1 mg of HexRu to 5 mL of the melted gel (150 °C). After homogenisation, 70 μL of HexRu-loaded gel was deposited on top of the 3D-printed electrode and left to gel for 10 min. The gel was prepared in a two-step process since HexRu has been shown to undergo reduction when exposed to temperature in aqueous solutions (Agarwal and Ganguli, 2014; Vijaikanth et al., 2013), hence disabling one-step preparation and posterior melting. The unused electrodes were covered in 100 μL of 2.5% w/v aqueous Miller LB broth and kept at 4 °C until use.

2.4. Bacterial suspensions and sample preparation

Trimethoprim-susceptible and resistant UTI *E. coli* strains (UPEC-29 and UPEC-3, respectively) were streaked out onto plates containing Miller LB media (2.5% w/v) and agar (1% w/v) from frozen glycerol stocks and grown at 37 °C overnight. Upon growth on LB/agar plates, single colonies were used to inoculate overnight cultures in 50 mL of Miller LB broth (2.5% w/v) at 37 °C under 150 rpm. Bacterial suspensions from overnight cultures were pipetted onto the gel-modified 3D-

printed electrodes and placed at 37 °C to perform the experiments. An analogous process was followed using *P. aeruginosa*. This process gives a starting bacterial concentration of ≈$3.5{\cdot}10^9$ CFU/mL. The samples were prepared as follows: for antibiotic-free baselines, 100 μL of aqueous Miller LB broth (aq. MLB) were used; for antibiotic-loaded baselines, 50 μL of aq. MLB and 50 μL of antibiotic-loaded aq. MLB broth were used. Amoxicillin, fosfomycin, and gentamicin (Merck, UK) were used at 8 μg/mL (minimum inhibitory concentration (MIC) (EUCAST, 2022),) in both susceptible and resistant *E. coli*, and gentamicin was used at 50 μg/mL and 40 μg/mL, respectively, in susceptible (PA14) and resistant (LESB58) *P. aeruginosa* (LaBauve and Wargo, 2012). Samples containing bacteria were prepared by pipetting 50 μL of aq. MLB and 50 μL of overnight grown bacteria, and bacteria-antibiotic samples were prepared by pipetting 50 μL of overnight grown bacteria and 50 μL of antibiotic in aq. MLB (Table SI in Supplementary Material, SM).

2.5. Electrochemical measurements and data analysis

Electrochemical measurements on the gel-modified 3D-printed electrodes were performed using a PalmSens PS4 potentiostat (PalmSens, Houten, Netherlands). Cyclic voltammograms (CV) were performed between −1.0 V and 0.5 V (scan rate 50 mV/s) prior to running the full script to determine the $E_{1/2}$ value and use it as a DC potential (E_{dc}) in the EIS measurements, which were performed from 0.1 Hz to 100 kHz at OCP of 0.3 V (acquired for 4 s). DPV measurements were performed across the same potential range as CV at a potential step of 0.1 V, pulse potential of 0.025 V, pulse time of 0.05 s, and scan rate of 1 V/s.

Impedance (Z), resistance (R), reactance (X), and negative phase (φ) were acquired from EIS measurements at 100 kHz, 10 kHz, 1 kHz, 100 Hz, 10 Hz, 1 Hz, and 0.1 Hz for 90 min in intervals of 5 min. We performed analyses over the initial and final 20 min of each sample (chosen since this is *E. coli*'s doubling time (Gibson et al., 2018)). Each measured value of Z, R, X, and φ at a given frequency was subtracted from the corresponding baseline measurement at each time step. Normalisation with respect to the maximum value within the time window of interest (in our case, initial and final 20 min of experiment) was performed to obtain values between 0 and 1 for all Z, R, X, and φ, and to correct for inter electrode variations of the signal. This process was followed at each scanned frequency (f), and the results at each time step were averaged over f. Values of 1 arising from this normalisation process were discarded. Following this approach, baseline measurements remain constant over time for all Z, R, X, and φ (see Fig. S1, SM). Each condition was tested in triplicate unless otherwise specified. We first proofed this data analysis process with results from previously published studies (Hannah et al., 2020b) before using it to assess the susceptibility of *E. coli* and *P. aeruginosa* against amoxicillin, fosfomycin, and gentamicin.

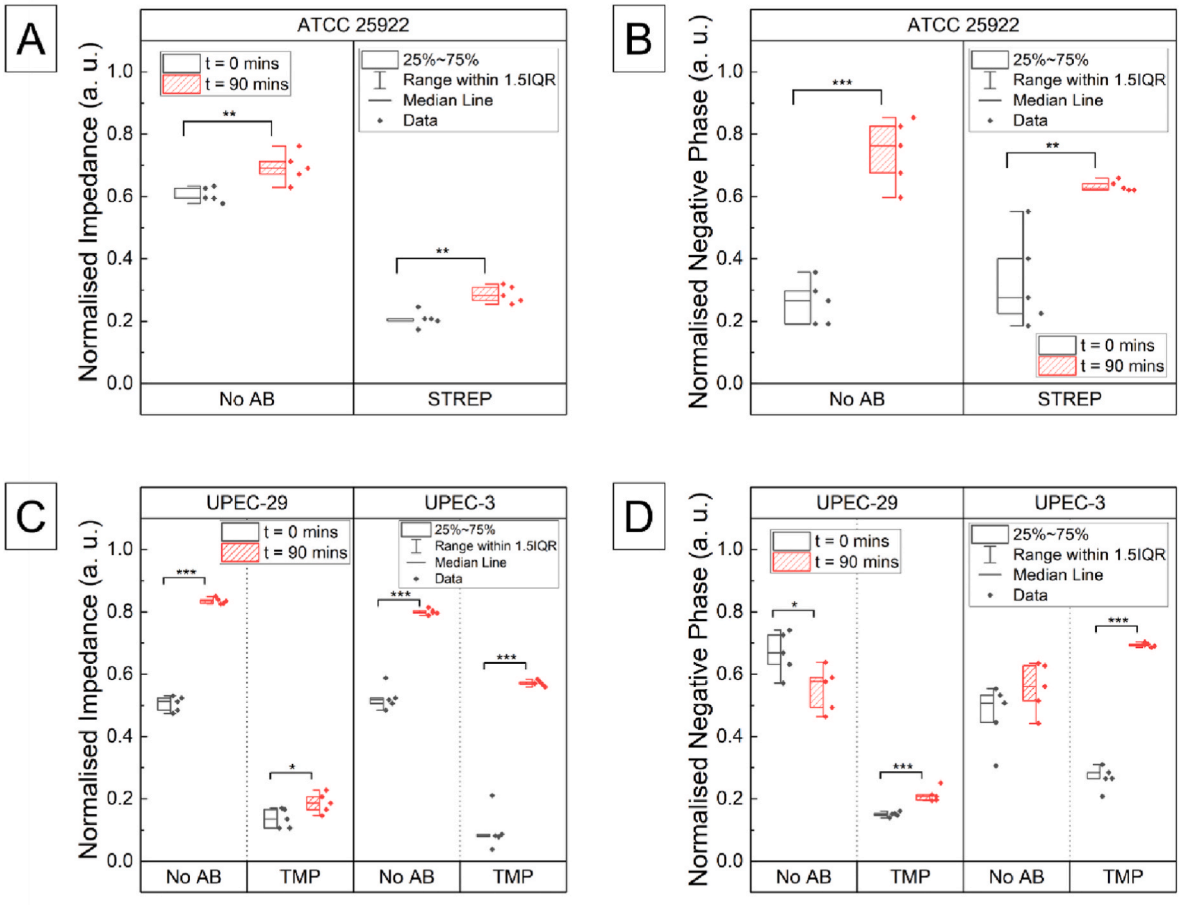

Fig. 2. (A) Normalised impedance and (B) normalised negative phase values for E. coli (ATCC 25922) and E. coli (ATCC 25922) with 4 μg/mL at 100 kHz (n = 5). (C) Normalised impedance and (D) normalised negative phase (data from (Hannah et al., 2020b)) for susceptible (UPEC-29) and resistant (UPEC-3) E. coli with and without 8 μg/mL of trimethoprim (TMP). Data averaged from 100 kHz to 10 Hz (n = 5). p-values obtained from paired student t-tests. Further statistical details are reported in Fig. S3 (Supplementary Material).

3. Results and discussion

3.1. Initial testing: E. coli on screen-printed electrodes

To develop the novel data analysis techniques reported in this work, we analysed the impedimetric growth data using *E. coli* ATCC 25922 (streptomycin-susceptible) (Hannah et al., 2020b), UPEC-29 (trimethoprim-susceptible – S), and UPEC-3 (trimethoprim-resistant – R) on gel-modified screen-printed electrodes (Fig. 2). These are both clinical UTI strains and were isolated for us by colleagues in the Department of Medical Microbiology, Glasgow, Royal Infirmary.

Fig. 2A and B show the time evolution of the normalised impedance (Z) and negative phase (φ), respectively at 100 kHz over the initial and final 20 min of measurement ($t = 0$ min and $t = 90$ min, respectively, for simplification). When comparing to the baseline evolution over time, where all parameters remain constant, there is a relative increase of Z over time for growing microorganisms, which contrasts with the sudden Z decrease when 4 μg/mL of streptomycin is added. This decrease in Z is associated with the action of streptomycin, which is a bactericidal antibiotic that kills cells by increasing the permeability of the cell membrane through ribosome-aminoglycoside interactions (Baquero and Levin, 2021). This enhancement of the cell membrane permeability, apart from leading to cellular death, disrupts normal ion transport through the cell membrane, leading to the release of Na^+ and Cl^- ions to the medium, thereby increasing the conductivity of the system and therefore decreasing total impedance over time. Fig. 2A also suggests that the biggest changes arising from the action of streptomycin take place over the first 20 min. Fig. 2B suggests that changes in φ can also be detected and associated to cellular growth/death. Unlike Z, changes in φ are not associated with the electrical properties of the cells but to their number instead. This cell number is given by initial cell seeding density and growth over time.

If the action of the used antibiotic is relatively slow, some bacterial growth may occur over the initial time course of the experiment, therefore inducing a lag into the measured signal. Once the bacterial cells die, their electrical properties change but they are still physically present in the system, therefore contributing to this phase lag. It can be noted, from Fig. 2B, that the induced lag in ATCC-25922 in the presence of streptomycin is lower than that in ATCC 25922 in the absence of streptomycin, supporting the hypothesis presented above. Nonetheless, given the relatively high cell density and the small size of the sample, φ values of *E. coli* in the presence of streptomycin are still relatively high.

Fig. 2C and D show the normalised impedance and negative phase, respectively, at 100 kHz and 10 Hz (averaged, $n = 5$) for UPEC-29 (S) and UPEC-3 (R). Trimethoprim, when used alone, is a bacteriostatic antibiotic that inhibits the reduction of dihydrofolate to tetrahydrofolate, which is required for bacterial growth (Maynard et al., 2018; T. R. Kemnic and Coleman, 2021). Fig. 2C suggests that growing cells lead to increasing values of Z, analogously to Fig. 2A, and that there are no significant changes between UPEC-29 and UPEC-3, which indicates that growth rates are similar when no antibiotic is present. When adding 8 μg/mL of trimethoprim to UPEC-29, there is a decrease in the normalised impedance over time, similar to that observed in Fig. 2A when using streptomycin. We found significantly reduced Z and φ median and mean values of trimethoprim over streptomycin (Table SIV, SM), indicating that this method could potentially allow clear differences between antibiotic mechanisms of action to be determined through interpretation of the impedimetric response. Therefore, more experiments are required to determine if the platform can discern between the use of different antibiotics. Conversely, addition of 8 μg/mL of trimethoprim to UPEC-3 produces a relative increase of Z over time, with a median considerably lower than bacteria growing in the absence of trimethoprim, but significantly higher than for dying bacteria, therefore indicating cellular growth at slower rates. Fig. 2C suggests that differences between cellular growth, inhibited growth, and death can be detected using the 3D-printed system from analysis of the median over time. Fig. 2D suggests that changes in φ can be detected between growing and dying bacteria, and that inhibited cellular growth provides different readings than growing cells.

This data analysis method demonstrates that it is possible to clearly differentiate between inhibited and uninhibited bacterial growth within 90 min using screen-printed, gel-modified electrodes (SPEs). This approach was applied using our 3D-printed electrochemical biosensor to confirm the observed trends and expand the investigation to resistance (R) and reactance (X) and increase the frequency window to obtain more information on the biological processes taking place. This approach provides a more cost-efficient, rapid method for AST analysis.

3.2. Escherichia coli: Fully 3D-printed sensor and platform

Fig. 3 shows the results of investigating how three different bactericidal antibiotics (amoxicillin, fosfomycin, and gentamicin, 8 μg/mL) affect UPEC-29 and UPEC-3 strains. Fig. 3A and B show, respectively, the normalised Z and R at $t = 0$ min and $t = 90$ min. Fig. 3A and B suggest that, in the absence of antibiotics, there is an increase of both the normalised Z and R, indicating that both strains grow at similar rates, which is in accordance with the results from Fig. 2. Over the first 20 min of the experiment, both UPEC-29 and UPEC-3 present considerable growth ($Z > 0.5$), but both strains appear to exhibit majority of growth after the initial 20 min (exponential growth). Fig. 3A shows increased Z of UPEC-3 in the presence of 8 μg/mL of gentamicin, suggesting that the UPEC-3 strain has developed a degree of resistance towards this antibiotic (since the same observation cannot be made for UPEC-29). Decreased Z values for UPEC-3 in the presence of gentamicin in Fig. 3A and B indicate a slow relative increase during the last 20 min, suggesting that most cellular growth occurs over the initial stages of the experiment. A similar observation can be made for UPEC-3 in the presence of 8 μg/mL of fosfomycin, which shows relatively high values of Z over time, which may suggest that a degree of resistance has been developed towards fosfomycin. For UPEC-29 in the presence of fosfomycin, most cellular inhibition takes place over the initial stage of the experiment, and a relative Z increase is observed towards the end of the experiment. Irrespective of whether there is cellular growth or death, the obtained results contrast with the baseline measurements, where constant values of Z, R, X, and φ are obtained over time.

Fig. 3B suggests that the resistance R is the most informative component of the impedimetric response and that most of the electrical characteristics of the cellular environment arise from the DC component. Analysis of the reactance X (Fig. S2A, SM) over time revealed a slight increase over time for strains without antibiotic, suggesting that as cells grow, they enhance the ability of the biomodified sensor surface to store charge, a trend that appears inverted in the presence of antibiotics. The ability to store charge is related to the number of cells present in the sample, and so X and φ may be better understood when analysed together (Fig. S2B, SM). Nevertheless, our data does not seem to provide enough statistical relevance to draw a significant conclusion towards charge storage and signal lag, suggesting that the 3D-printed platform does not provide enough information about changes in X and φ. These limitations are hypothesised to arise from two main factors: (i) all three electrodes are made of CB-PLA as opposed to using an Ag/AgCl reference, which would improve precision, and (ii) the low CB doping of the CB-PLA commercial material, which limits the current that can be driven through the electrode. Nevertheless, our results suggest that Z and R readings are adequate for rapid assessment of bacterial growth and death.

3.3. Pseudomonas aeruginosa

As a final experiment, we studied a different bacterial strain to demonstrate that this platform can be used for different types of bacterial infections. Fig. 4 shows the results obtained from analysing gentamicin-susceptible and resistant strains of *P. aeruginosa* (PA14 and

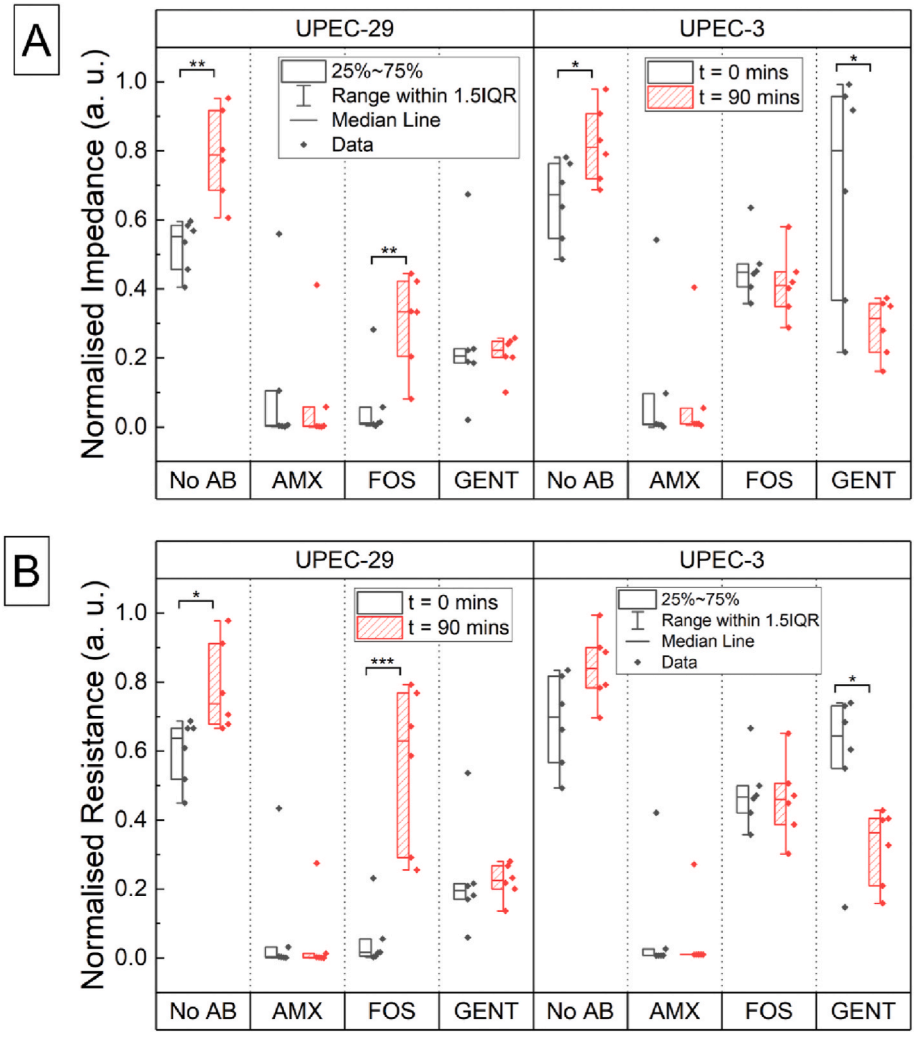

Fig. 3. (A) Normalised impedance, and (B) normalised resistance over the first and last 20 min (t = 0 and t = 90 min for simplicity), respectively, for UPEC-29 and UPEC-3 E. coli strains in the presence and absence of 8 μg/mL of amoxicillin, fosfomycin, and gentamicin (n = 6). Each point shown in the graph is an average over all the studied frequencies (100 kHz, 10 kHz, 1 kHz, 100 Hz, 10 Hz, 1 Hz, and 0.1 Hz). p-values obtained from paired student t-tests. Further statistical details are reported in Fig. S4 (Supplementary Material).

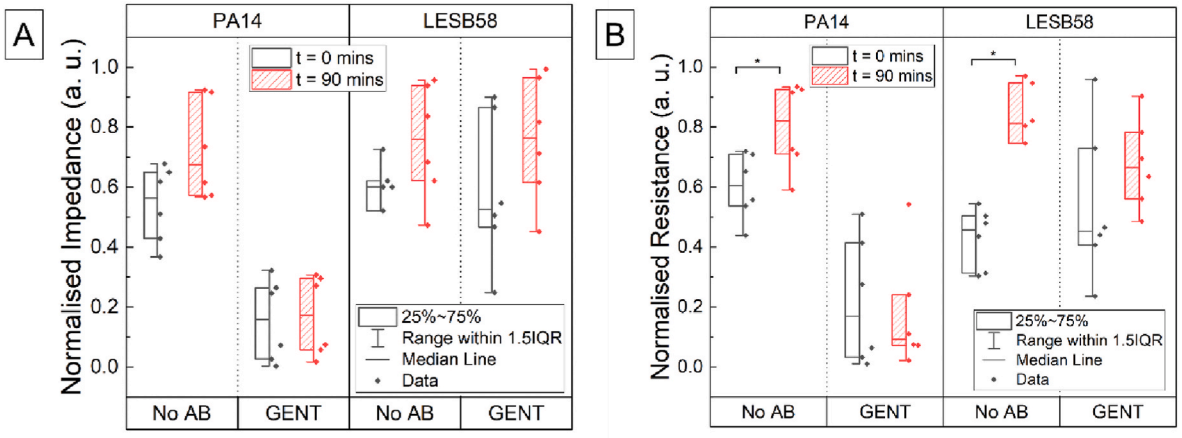

Fig. 4. (A) Normalised impedance, and (B) normalised resistance over the first and last 20 min (t = 0 and t = 90 min for simplicity), respectively, for PA14 and LESB58 P. aeruginosa strains in the presence and absence of 40 μg/mL of gentamicin. Data averaged over all the studied frequencies (100 kHz, 10 kHz, 1 kHz, 100 Hz, 10 Hz, 1 Hz, and 0.1 Hz), n = 3. p-values obtained from paired student t-tests. Further statistical details are reported in Fig. S6 (Supplementary Material).

LESB58, respectively (O'Brien et al., 2017)) in the presence and absence of gentamicin. Analogously to Figs. 2 and 3, we observed an increase in *Z* and *R* over time (Fig. 4A and B, respectively) in the absence of antibiotic. The same is observed for LESB58, while the opposite trend is observed for PA14 when an antibiotic is present. These results are consistent with those in Figs. 2 and 3. Analogously to the observations made in UPEC-29 and UPEC-3, an increase of *X* can be induced over time when measuring PA14 and LESB58 in the 3D-printed biosensor in the absence of

antibiotic (Fig. S3A, SM). These results suggest that cellular growth enhances the ability of the system to store charge and relates to the number of cells present in the sample, which lead to higher current lags (Fig. S3B, SM). This trend is reversed in the presence of antibiotic, and consistent with the results obtained from UPEC-29 and UPEC-3 strains. Notwithstanding, the data acquired in the 3D-printed biosensor does not seem to provide enough statistical significance to draw conclusive remarks about how *P. aeruginosa* bacterial growth and inhibition influence X and φ readings, therefore requiring further evaluation. Analogously to the *E. coli* studies, though, our measurements indicate that Z and R measurements are enough to infer bacterial growth and inhibition, reliably, in just 90 min.

Fig. 4 showed stronger statistical relevance between the different datasets towards the final stages of the experiment (Fig. S5 SM). This is associated to the fact that *P. aeruginosa* strains are slower growing organisms than *E. coli* (~30 min for PA14 and ~45 min for LESB58), so time-to-result may be slightly increased because of this factor. While it appears in Fig. 4 that cellular death can be induced in only 20 min, it may be more appropriate to analyse the data over doubling times of the studied strain. Additionally, *P. aeruginosa* strains are known for producing pyocyanin and pyoverdine. The former is a metabolite that has the ability to oxidise and reduce other molecules, a process that may be electrically competing with bacterial growth, therefore hindering part of the signal and challenging rapid diagnosis of cellular growth/inhibition. *P. aeruginosa* can dispose of excess electrons by producing pyocyanin (Rabaey et al., 2005), which would tend to decrease Z and R as opposed to their increase associated to cellular growth form our data analysis. Similarly, pyoverdine is a siderophore generated during growth (O'Brien et al., 2017), leading to an increase of conductivity on the surface electrode that competes with the Z increase associated to cellular growth, therefore requiring longer experiment times to reliably assess bacterial growth.

4. Conclusions

We have demonstrated that by combining a novel data analysis method, EIS monitoring and a fully 3D-printed electrochemical biosensor, inhibited or uninhibited bacterial growth can be determined in clinically useful timeframes. This approach associates cellular growth to relative increases (from 0 to 1) of Z and R over time, and produces conclusive data in 90 min. This data analysis method provides constant values over time for baseline measurements, and as such, bacterial growth and death can be induced through normalisation with respect to the corresponding baseline. We have used this data analysis method to our previous work to ensure its feasibility and provide meaning to 0 (cellular death) and 1 (bacterial growth) values. We have exploited multi-material 3D-printing advances to develop a fully 3D-printed, gel-modified electrochemical sensor that supports prokaryotic cell adhesion and can be used to induce cellular growth and death. This platform, combined with our novel data analysis, suggests that it is possible to study the effects of different antibiotics on different microorganisms, and shows clear identification of bacterial growth. For *E. coli*, amoxicillin provides similar readings between the baseline measurements and the measurements in the presence of bacterial strains. In all experiments, a decrease of both the normalised Z and R is observed. However, lower readings in the presence of both UPEC-29 and UPEC-3 strains are obtained when compared to the baseline measurements. Since baseline values of normalised Z and R are low in the presence of amoxicillin, the relative decrease in both Z and R will also be low, reaching 0 very quickly. It must be noted that this value of 0 is never reached in the baseline experiments, and together with a no increase of Z and R, the results suggest that amoxicillin is indeed contributing to cellular death in both UPEC-29 and UPEC-3 strains (see Table SI, SM, Fig. 3, and Fig. S1, SM). Notwithstanding, more measurements may be required to strengthen this conclusion. Fosfomycin seems to be ineffective in UPEC-29, but it appears to be inhibiting bacterial growth in UPEC-3, while gentamicin seems to inhibit growth in UPEC-29 but and be very efficient in UPEC-3 (Fig. 3). Similarly, gentamicin is effective on PA14, but not on LESB58 (Fig. 4). We also studied the evolution of X and φ in these systems. While more measurements are needed, X seems to increase with growing cells and vice versa, and φ appears to remain relatively constant between the initial and final stages of the experiment in 3D-printed systems. Nonetheless, with screen-printed electrode measurements, φ clearly increases with growing cells since higher numbers induce bigger signal lags that are picked up by the sensor. This trend is not observed on 3D-printed systems, likely for two reasons: (i) use of the same material in all electrodes (reference, counter, and working), and (ii) low CB loading from the commercially available PLA. This can be addressed in the future by developing our own 3D-printing filaments where the composition of the material can be fully controlled. Another option is to use resin-based approaches rather than filament-based 3D-printing, since higher electrode resolutions can be achieved.

All in all, we have demonstrated the use of multi-material 3D-printing to rapidly tackle AST in two species of Gram-negative bacteria. We have shown that our data analysis method can be applied in a variety of conditions, using different types of electrodes (gold-based SPEs and carbon-based 3D-printed), different mediators (potassium ferricyanide and potassium ferrocyanide, and hexaammineruthenium (III) chloride), and different bacterial strains. We have successfully demonstrated the effect of different bactericidal antibiotics on different ESKAPE pathogens, and we aim to study Gram-positive strains to strengthen species differentiation capabilities. From initial testing, our results suggest that, with further testing, impedimetric differences could be detected between bactericidal and bacteriostatic antibiotics. Hence, we aim to further investigate this effect in order to establish clear differences between their mechanism of action and provide, in the future, efficient and rapid diagnostics.

CRediT authorship contribution statement

R. Domingo-Roca: Conceptualization, Data curation, Formal analysis, Investigation, Methodology, Writing – original draft. **P. Lasserre:** Data curation, Formal analysis, Methodology, Writing – review & editing. **L. Riordan:** Data curation, Methodology, Writing – review & editing. **A.R. Macdonald:** Data curation, Formal analysis. **A. Dobrea:** Data curation. **K.R. Duncan:** Supervision. **S. Hannah:** Resources, Conceptualization, Funding acquisition. **M. Murphy:** Resources. **P.A. Hoskisson:** Resources. **D.K. Corrigan:** Conceptualization, Data curation, Formal analysis, Funding acquisition, Investigation, Methodology, Supervision, Writing – review & editing.

Declaration of competing interest

The authors declare that they have no known competing financial interests or personal relationships that could have appeared to influence the work reported in this paper.

Data availability

Data will be made available on request.

Acknowledgments

The authors would like to thank the Scottish Enterprise High Growth Spinout Project and Microplate Dx for project funding, the NHS Greater Glasgow & Clyde for providing clinical support, and the Engineering and Physical Sciences Research Council (EPSRC) [grant number EP/W006456/1].

Appendix A. Supplementary data

Supplementary data to this article can be found online at https://doi.

org/10.1016/j.biosx.2023.100308.

References

Agarwal, S., Ganguli, J.N., 2014. Hydrogenation by nanoscale ruthenium embedded into the nanopores of K-10 clay. RSC Adv. 4, 11893 https://doi.org/10.1039/c3ra47162d.

Anahtar, M.N., Yang, J.H., Kanjilal, S., 2021. Applications of machine learning to the problem of antimicrobial resistance: an emerging model for translational research. J. Clin. Microbiol. 59 https://doi.org/10.1128/JCM.01260-20 e01260-20.

Baltekin, Ö., Boucharin, A., Tano, E., Andersson, D.I., Elf, J., 2017. Antibiotic susceptibility testing in less than 30 min using direct single-cell imaging. Proc. Natl. Acad. Sci. U.S.A. 114, 9170–9175. https://doi.org/10.1073/pnas.1708558114.

Baquero, F., Levin, B.R., 2021. Proximate and ultimate causes of the bactericidal action of antibiotics. Nat. Rev. Microbiol. 19, 123–132. https://doi.org/10.1038/s41579-020-00443-1.

Behera, B., Anil Vishnu, G.K., Chatterjee, S., Sitaramgupta V, V.S.N., Sreekumar, N., Nagabhushan, A., Rajendran, N., Prathik, B.H., Pandya, H.J., 2019. Emerging technologies for antibiotic susceptibility testing. Biosens. Bioelectron. 142, 111552 https://doi.org/10.1016/j.bios.2019.111552.

Brosel-Oliu, S., Mergel, O., Uria, N., Abramova, N., van Rijn, P., Bratov, A., 2019a. 3D impedimetric sensors as a tool for monitoring bacterial response to antibiotics. Lab Chip 19, 1436–1447. https://doi.org/10.1039/C8LC01220B.

Brosel-Oliu, S., Mergel, O., Uria, N., Abramova, N., van Rijn, P., Bratov, A., 2019b. 3D impedimetric sensors as a tool for monitoring bacterial response to antibiotics. Lab Chip 19, 1436–1447. https://doi.org/10.1039/C8LC01220B.

Butler, D., Goel, N., Goodnight, L., Tadigadapa, S., Ebrahimi, A., 2019. Detection of bacterial metabolism in lag-phase using impedance spectroscopy of agar-integrated 3D microelectrodes. Biosens. Bioelectron. 129, 269–276. https://doi.org/10.1016/j.bios.2018.09.057.

Cardoso, R.M., Silva, P.R.L., Lima, A.P., Rocha, D.P., Oliveira, T.C., do Prado, T.M., Fava, E.L., Fatibello-Filho, O., Richter, E.M., Muñoz, R.A.A., 2020. 3D-Printed graphene/polylactic acid electrode for bioanalysis: biosensing of glucose and simultaneous determination of uric acid and nitrite in biological fluids. Sensor. Actuator. B Chem. 307, 127621 https://doi.org/10.1016/j.snb.2019.127621.

Derzsi, L., Kaminski, T.S., Garstecki, P., 2016. Antibiograms in five pipetting steps: precise dilution assays in sub-microliter volumes with a conventional pipette. Lab Chip 16, 893–901. https://doi.org/10.1039/C5LC01151E.

Domingo-Roca, R., Macdonald, A.R., Hannah, S., Corrigan, D.K., 2022. Integrated multi-material portable 3D-printed platform for electrochemical detection of dopamine and glucose. Analyst 147, 4598–4606. https://doi.org/10.1039/D2AN00862A.

Elyan, E., Hussain, A., Sheikh, A., Elmanama, A.A., Vuttipittayamongkol, P., Hijazi, K., 2022. Antimicrobial resistance and machine learning: challenges and opportunities. IEEE Access 10, 31561–31577. https://doi.org/10.1109/ACCESS.2022.3160213.

Etayash, H., Khan, M.F., Kaur, K., Thundat, T., 2016. Microfluidic cantilever detects bacteria and measures their susceptibility to antibiotics in small confined volumes. Nat. Commun. 7, 12947 https://doi.org/10.1038/ncomms12947.

EUCAST, 2022. The European Committee on Antimicrobial Susceptibility Testing. Routine and Extended Internal Quality Control for MIC Determination and Disk Diffusion as Recommended by EUCAST.

Felice, C.J., Madrid, R.E., Olivera, J.M., Rotger, V.I., Valentinuzzi, M.E., 1999. Journal of microbiological methods. J. Microbiol. Methods 6.

Gibson, B., Wilson, D.J., Feil, E., Eyre-Walker, A., 2018. The Distribution of Bacterial Doubling Times in the Wild 9. https://doi.org/10.1101/214783.

Gnaim, R., Golberg, A., Sheviryov, J., Rubinsky, B., González, C.A., 2020. Detection and differentiation of bacteria by electrical bioimpedance spectroscopy. Biotechniques 69, 26–36. https://doi.org/10.2144/btn-2019-0080.

Gómez, R., 2002. Microscale electronic detection of bacterial metabolism. Sensor. Actuator. B Chem. 86, 198–208. https://doi.org/10.1016/S0925-4005(02)00175-2.

Gumbo, T., Siyambalapitiyage Dona, C.S.W., Meek, C., Leff, R., 2009. Pharmacokinetics-pharmacodynamics of pyrazinamide in a novel in vitro model of tuberculosis for sterilizing effect: a paradigm for faster assessment of new antituberculosis drugs. Antimicrob. Agents Chemother. 53, 3197–3204. https://doi.org/10.1128/AAC.01681-08.

Hannah, S., Addington, E., Alcorn, D., Shu, W., Hoskisson, P.A., Corrigan, D.K., 2019. Rapid antibiotic susceptibility testing using low-cost, commercially available screen-printed electrodes. Biosens. Bioelectron. 145, 111696 https://doi.org/10.1016/j.bios.2019.111696.

Hannah, S., Al-Hatmi, M., Gray, L., Corrigan, D.K., 2020a. Low-cost, thin-film, mass-manufacturable carbon electrodes for detection of the neurotransmitter dopamine. Bioelectrochemistry 133, 107480. https://doi.org/10.1016/j.bioelechem.2020.107480.

Hannah, S., Dobrea, A., Lasserre, P., Blair, E.O., Alcorn, D., Hoskisson, P.A., Corrigan, D. K., 2020b. Development of a rapid, antimicrobial susceptibility test for E. coli based on low-cost, screen-printed electrodes. Biosensors 10, 153. https://doi.org/10.3390/bios10110153.

Hannah, S., Domingo-Roca, R., Hoskisson, P.A., Murphy, M.E., Corrigan, D.K., 2022. Electrochemical antibiotic susceptibility testing: an emerging approach for fast and accurate determination of antibiotic effect in complex samples. Curr. Opin. Electrochem. 35, 101033 https://doi.org/10.1016/j.coelec.2022.101033.

Hatada, M., Loew, N., Inose-Takahashi, Y., Okuda-Shimazaki, J., Tsugawa, W., Mulchandani, A., Sode, K., 2018. Development of a glucose sensor employing quick and easy modification method with mediator for altering electron acceptor preference. Bioelectrochemistry 121, 185–190. https://doi.org/10.1016/j.bioelechem.2018.02.001.

Johnson, W.L., France, D.C., Rentz, N.S., Cordell, W.T., Walls, F.L., 2017. Sensing bacterial vibrations and early response to antibiotics with phase noise of a resonant crystal. Sci. Rep. 7, 12138 https://doi.org/10.1038/s41598-017-12063-6.

Kemnic, T.R., Coleman, M., 2021. Trimethoprim sulfamethoxazole. Trimethoprim sulfamethoxazole. URL. https://www.ncbi.nlm.nih.gov/books/NBK513232/.

Khaledi, A., Weimann, A., Schniederjans, M., Asgari, E., Kuo, T., Oliver, A., Cabot, G., Kola, A., Gastmeier, P., Hogardt, M., Jonas, D., Mofrad, M.R., Bremges, A., McHardy, A.C., Häussler, S., 2020. Predicting antimicrobial resistance in *Pseudomonas aeruginosa* with machine learning-enabled molecular diagnostics. EMBO Mol. Med. 12 https://doi.org/10.15252/emmm.201910264.

Kodan, L.R., Verschueren, K.J.C., Kanhai, H.H.H., van Roosmalen, J.J.M., Bloemenkamp, K.W.M., Rijken, M.J., 2018. The golden hour of sepsis: an in-depth analysis of sepsis-related maternal mortality in middle-income country Suriname. PLoS One 13, e0200281. https://doi.org/10.1371/journal.pone.0200281.

Kumar, Anand, Roberts, D., Wood, K., Light, B., Parrillo, J.E., Shandra, S., Suppes, R., Feinstein, D., Zanotti, S., Taiberg, L., Gurka, D., Kumar, Aseem, Cheang, M., 2006. Duration of hypotension before initiation of effective antimicrobial therapy is the critical determinant of survival in human septic shock. Crit. Care Med. 34, 1589–1596. https://doi.org/10.1097/01.CCM.0000217961.75225.E9.

LaBauve, A.E., Wargo, M.J., 2012. Growth and laboratory maintenance of *Pseudomonas aeruginosa*. Curr. Proto. in Microbiol. 25 https://doi.org/10.1002/9780471729259.mc06e01s25.

Manzanares Palenzuela, C.L., Novotný, F., Krupička, P., Sofer, Z., Pumera, M., 2018. 3D-Printed graphene/polylactic acid electrodes promise high sensitivity in electroanalysis. Anal. Chem. 90, 5753–5757. https://doi.org/10.1021/acs.analchem.8b00083.

Martins, S.B., Selby, M.J., 1980. Evaluation of a rapid method for the quantitative estimation of coliforms in meat by impedimetric procedures. Appl. Environ. Microbiol. 39, 518–524. https://doi.org/10.1128/aem.39.3.518-524.1980.

Maynard, C., Cummins, I., Green, J., Weinkove, D., 2018. A bacterial route for folic acid supplementation. BMC Biol. 16, 67. https://doi.org/10.1186/s12915-018-0534-3.

McLean, C., Tiller, B., Mansour, R., Brown, K., Windmill, J., Dennany, L., 2022. Characterising the response of novel 3D printed CNT electrodes to the virulence factor pyocyanin. J. Electroanal. Chem. 909, 116149 https://doi.org/10.1016/j.jelechem.2022.116149.

Miller, C., Stiglich, M., Livingstone, M., Gilmore, J., 2019. Impedance-based biosensing of Pseudomonas putida via solution blow spun PLA: MWCNT composite nanofibers. Micromachines 10, 876. https://doi.org/10.3390/mi10120876.

Muhsin, S.A., Al-Amidie, M., Shen, Z., Mlaji, Z., Liu, J., Abdullah, A., El-Dweik, M., Zhang, S., Almasri, M., 2022. A microfluidic biosensor for rapid simultaneous detection of waterborne pathogens. Biosens. Bioelectron. 203, 113993 https://doi.org/10.1016/j.bios.2022.113993.

Murray, C.J., Ikuta, K.S., Sharara, F., Swetschinski, L., Robles Aguilar, G., Gray, A., Han, C., Bisignano, C., Rao, P., Wool, E., Johnson, S.C., Browne, A.J., Chipeta, M.G., Fell, F., Hackett, S., Haines-Woodhouse, G., Kashef Hamadani, B.H., Kumaran, E.A. P., McManigal, B., Agarwal, R., Akech, S., Albertson, S., Amuasi, J., Andrews, J., Aravkin, A., Ashley, E., Bailey, F., Baker, S., Basnyat, B., Bekker, A., Bender, R., Bethou, A., Bielicki, J., Boonkasidecha, S., Bukosia, J., Carvalheiro, C., Castañeda-Orjuela, C., Chansamouth, V., Chaurasia, S., Chiurchiù, S., Chowdhury, F., Cook, A. J., Cooper, B., Cressey, T.R., Criollo-Mora, E., Cunningham, M., Darboe, S., Day, N.P. J., De Luca, M., Dokova, K., Dramowski, A., Dunachie, S.J., Eckmanns, T., Eibach, D., Emami, A., Feasey, N., Fisher-Pearson, N., Forrest, K., Garrett, D., Gastmeier, P., Giref, A.Z., Greer, R.C., Gupta, V., Haller, S., Haselbeck, A., Hay, S.I., Holm, M., Hopkins, S., Iregbu, K.C., Jacobs, J., Jarovsky, D., Javanmardi, F., Khorana, M., Kissoon, N., Kobeissi, E., Kostyanev, T., Krapp, F., Krumkamp, R., Kumar, A., Kyu, H. H., Lim, C., Limmathurotsakul, D., Loftus, M.J., Lunn, M., Ma, J., Mturi, N., Munera-Huertas, T., Musicha, P., Mussi-Pinhata, M.M., Nakamura, T., Nanavati, R., Nangia, S., Newton, P., Ngoun, C., Novotney, A., Nwakanma, D., Obiero, C.W., Olivas-Martinez, A., Olliaro, P., Ooko, E., Ortiz-Brizuela, E., Peleg, A.Y., Perrone, C., Plakkal, N., Ponce-de-Leon, A., Raad, M., Ramdin, T., Riddell, A., Roberts, T., Robotham, J.V., Roca, A., Rudd, K.E., Russell, N., Schnall, J., Scott, J.A.G., Shivamallappa, M., Sifuentes-Osornio, J., Steenkeste, N., Stewardson, A.J., Stoeva, T., Tasak, N., Thaiprakong, A., Thwaites, G., Turner, C., Turner, P., van Doorn, H.R., Velaphi, S., Vongpradith, A., Vu, H., Walsh, T., Waner, S., Wangrangsimakul, T., Wozniak, T., Zheng, P., Sartorius, B., Lopez, A.D., Stergachis, A., Moore, C., Dolecek, C., Naghavi, M., 2022. Global burden of bacterial antimicrobial resistance in 2019: a systematic analysis. Lancet 399, 629–655. https://doi.org/10.1016/S0140-6736(21)02724-0.

Musuka, S., Srivastava, S., Siyambalapitiyage Dona, C.W., Meek, C., Leff, R., Pasipanodya, J., Gumbo, T., 2013. Thioridazine pharmacokinetic-pharmacodynamic parameters "Wobble" during treatment of tuberculosis: a theoretical basis for shorter-duration curative monotherapy with congeners. Antimicrob. Agents Chemother. 57, 5870–5877. https://doi.org/10.1128/AAC.00829-13.

O'Brien, S., Williams, D., Fothergill, J.L., Paterson, S., Winstanley, C., Brockhurst, M.A., 2017. High virulence sub-populations in Pseudomonas aeruginosa long-term cystic fibrosis airway infections. BMC Microbiol. 17, 30. https://doi.org/10.1186/s12866-017-0941-6.

O'Neill, J., 2014. Antimicrobial Resistance: Tackling a Crisis for the Health and Wealth of Nations.

Qiu, W., Nagl, S., 2021. Automated miniaturized digital microfluidic antimicrobial susceptibility test using a chip-integrated optical oxygen sensor. ACS Sens. 6, 1147–1156. https://doi.org/10.1021/acssensors.0c02399.

Rabaey, K., Boon, N., Höfte, M., Verstraete, W., 2005. Microbial phenazine production enhances electron transfer in biofuel cells. Environ. Sci. Technol. 39, 3401–3408. https://doi.org/10.1021/es048563o.

Ramiah Rajasekaran, P., Chapin, A.A., Quan, D.N., Herberholz, J., Bentley, W.E., Ghodssi, R., 2020. 3D-Printed electrochemical sensor-integrated transwell systems. Microsyst Nanoeng 6, 100. https://doi.org/10.1038/s41378-020-00208-z.

Rengaraj, S., Cruz-Izquierdo, Á., Scott, J.L., Di Lorenzo, M., 2018. Impedimetric paper-based biosensor for the detection of bacterial contamination in water. Sensor. Actuator. B Chem. 265, 50–58. https://doi.org/10.1016/j.snb.2018.03.020.

Richter, E.M., Rocha, D.P., Cardoso, R.M., Keefe, E.M., Foster, C.W., Munoz, R.A.A., Banks, C.E., 2019. Complete additively manufactured (3D-printed) electrochemical sensing platform. Anal. Chem. 91, 12844–12851. https://doi.org/10.1021/acs.analchem.9b02573.

Sebechlebská, T., Vaněčková, E., Choińska-Młynarczyk, M.K., Navrátil, T., Poltorak, L., Bonini, A., Vivaldi, F., Kolivoška, V., 2022. 3D printed platform for impedimetric sensing of liquids and microfluidic channels. Anal. Chem. 94, 14426–14433. https://doi.org/10.1021/acs.analchem.2c03191.

Siller, I.G., Preuss, J.-A., Urmann, K., Hoffmann, M.R., Scheper, T., Bahnemann, J., 2020. 3D-Printed flow cells for aptamer-based impedimetric detection of E. coli crooks strain. Sensors 20, 4421. https://doi.org/10.3390/s20164421.

Son, K., Stocker, R., 2019. (73) Assignee, vol. 38. PhAST Corp., Boston,MA (US.

Swami, P., Sharma, A., Anand, S., Gupta, S., 2021. DEPIS: a combined dielectrophoresis and impedance spectroscopy platform for rapid cell viability and antimicrobial susceptibility analysis. Biosens. Bioelectron. 182, 113190 https://doi.org/10.1016/j.bios.2021.113190.

Swami, P., Verma, G., Holani, A., Kamaraju, S., Manchanda, V., Sritharan, V., Gupta, S., 2022. Rapid antimicrobial susceptibility profiling using impedance spectroscopy. Biosens. Bioelectron. 200, 113876 https://doi.org/10.1016/j.bios.2021.113876.

Tang, Y., Zhen, L., Liu, J., Wu, J., 2013. Rapid antibiotic susceptibility testing in a microfluidic pH sensor. Anal. Chem. 85, 2787–2794. https://doi.org/10.1021/ac303282j.

van Belkum, A., Burnham, C.-A.D., Rossen, J.W.A., Mallard, F., Rochas, O., Dunne, W.M., 2020. Innovative and rapid antimicrobial susceptibility testing systems. Nat. Rev. Microbiol. 18, 299–311. https://doi.org/10.1038/s41579-020-0327-x.

Vasala, A., Hytönen, V.P., Laitinen, O.H., 2020. Modern tools for rapid diagnostics of antimicrobial resistance. Front. Cell. Infect. Microbiol. 10, 308. https://doi.org/10.3389/fcimb.2020.00308.

Vijaikanth, V., Li, G., Swaddle, T.W., 2013. Kinetics of reduction of aqueous hexaammineruthenium(III) ion at Pt and Au microelectrodes: electrolyte, temperature, and pressure effects. Inorg. Chem. 52, 2757–2768. https://doi.org/10.1021/ic400062b.

Walker, K., Ripandelli, N., Flint, S., 2005. Rapid enumeration of Bifidobacterium lactis in milk powders using impedance. Int. Dairy J. 15, 183–188. https://doi.org/10.1016/j.idairyj.2004.06.004.

Wang, R., Wang, L., Yan, J., Luan, D., Tao sun, Wu, J., Bian, X., 2021. Rapid, sensitive and label-free detection of pathogenic bacteria using a bacteria-imprinted conducting polymer film-based electrochemical sensor. Talanta 226, 122135. https://doi.org/10.1016/j.talanta.2021.122135.

Ward, A.C., Hannah, A.J., Kendrick, S.L., Tucker, N.P., MacGregor, G., Connolly, P., 2018. Identification and characterisation of Staphylococcus aureus on low cost screen printed carbon electrodes using impedance spectroscopy. Biosens. Bioelectron. 110, 65–70. https://doi.org/10.1016/j.bios.2018.03.048.

World Health Organization, 2015. GLOBAL ACTION PLAN ON ANTIMICROBIAL RESISTANCE.